Iranian Journal of Microbiology
Volume 18 Number 4 (August 2026) 584-594
DOI: http://doi.org/10.18502/ijm.v18i4.22201

ORIGINAL ARTICLE

Antiviral activity of biogenic silver nanoparticles against HSV-1: integrating computational modeling and experimental validation

Mahsa Soltani[1], Ameneh Elikaei[1*], Parinaz Ghadam[2], Sona Ayadi Hassan[2]

[1]Department of Microbiology, Faculty of Biological Sciences, Alzahra University, Tehran, Iran
[2]Department of Biotechnology, Faculty of Biological Sciences, Alzahra University, Tehran, Iran

Received: January 2025**, Accepted:** May 2026

ABSTRACT

Background and Objectives: This study aimed to investigate the effects of biogenic silver nanoparticles (AgNPs) on Herpes simplex virus type 1 (HSV-1), focusing on the influence of plant-derived capping agents and their metal cores on antiviral efficacy and mechanism of action.

Materials and Methods: Biosynthesized AgNPs using aqueous extracts of *Juglans regia* (*J. regia*) and *Malva sylvestris* (*M. sylvestris*) were characterized, and their zeta potential was assessed. Molecular docking studies were performed to illuminate the interaction between AgNPs and viral particles. The antiviral activity was evaluated using viral titer quantification and a cytotoxicity assay, both performed on Vero cells.

Results: AgNPs exhibited zeta potentials of -8.87 mV and -5.49 mV for *J. regia* and *M. sylvestris*, respectively, indicating their stability and potential for interaction with viral particles. Strong binding affinities between AgNPs and viral glycoprotein D (gD) were revealed by molecular docking, which obtained negative MolDock scores. The antiviral assays demonstrated a ten-thousand-fold reduction in viral titers.

Conclusion: This research underscores the critical roles of capping agents and the metallic core in modulating the antiviral efficacy of plant-derived AgNPs against *HSV-1*, establishing them as a promising platform for novel antiviral therapeutics.

Keywords: Antiviral agents; Herpes simplex virus type 1; Metal nanoparticles; Molecular docking; Plant extracts

INTRODUCTION

One of the primary causes of infectious diseases, responsible for more than 20% of deaths worldwide, is viruses, which account for one-third of these deaths (1). The ongoing emergence and reemergence of viral infectious diseases will continue to significantly impact public health, microbiology, and related scientific fields, along with the unpredictability of epidemic occurrences (2). However, only a few viral diseases currently have available vaccines or antiviral medications, and some viruses are becoming resistant to these treatments (3). In this regard, studies on novel antiviral medications or strategies, such as nanoparticles (NPs), and on assessing their efficacy have become increasingly significant. The urgent need for dynamic and innovative antiviral drug development is clear, as viral diseases have caused millions of human fatalities worldwide over the course of human civilization (4).

HSV-1 is a common infectious agent that affects people of all age groups worldwide. The virus can

*Corresponding author: Ameneh Elikaei, Ph.D, Department of Microbiology, Faculty of Biological Sciences, Alzahra University, Tehran, Iran. Tel: +98-9126398037 Fax: +98-2188058912 Email: a.elikaei@alzahra.ac.ir

cause a variety of clinical manifestations, including asymptomatic cases, severe encephalitis, and even Alzheimer's disease. HSV-1, a member of the *Herpesviridae* family, has a linear double-stranded DNA genome that is enclosed within an icosahedral capsid. A proteinaceous layer, called the tegument, protects the icosahedral capsid, which is enveloped in a lipid membrane containing viral glycoproteins. Viral glycoproteins are essential for the virus to attach to and enter human cells (5). This virus is examined as a representative of viruses that have an envelope and utilize DNA as their genetic material.

NPs have become promising antimicrobial agents due to their advantageous characteristics, including a high surface-to-volume ratio, tunable charge, size, and shape, and their capacity to deliver substantial amounts of antibiotics or other therapeutic agents (6). Metallic NPs, including AgNPs, have attracted considerable attention for various applications, particularly in antibacterial applications, due to their exceptional physicochemical and optoelectronic properties. To address concerns about synthesis (hazardous solvents, precursors, and toxic byproducts), biological synthesis methods—often using microbial, plant, or biologically active agents—have gained increasing importance (7). The biosynthesized metallic NPs consist of a core and a cap, with biological material contributing to both the core formation and the surface capping.

AgNPs are classified by composition and oxidation state into AgO, Ag_2S, AgCl, Ag_3PO_4, AgBr, and AgI, plus a multi-oxide group AgO/ Ag_2O/ Ag_2O_3 / Ag_3O_4 / Ag_4O_4 treated as a single category (8). Together, these eight distinct forms underpin a range of antibacterial and other biotechnological applications. AgNPs can undergo various chemical modifications; the extent and type of these modifications depend on their properties. Chemical processes can modify their surface properties. In addition, AgNPs can aggregate, a process that may be modified by their coating agents (1, 9). It has been proposed that there is a direct relationship between the toxicity of AgNPs and their surface chemistry. AgNPs toxicity increases with positive increase in the zeta potential, which reflects a reduction in negative surface charge and a corresponding diminishment of the electrostatic barrier. This reduction facilitates closer contact and interaction between virus particles and AgNPs, leading to greater toxicity and a more pronounced antiviral effect. Additionally, the repulsive forces acting on virus particles at the outset can transition to attractive interactions when exposed to positively charged AgNPs, further promoting virus-AgNPs interactions. The toxicological mechanisms of NPs may encompass both physical and chemical interactions. The capping agents influence antimicrobial properties of AgNPs, including their antiviral activity, and also make them more stable (1). This study evaluates the antiviral effects of NPs against HSV-1 through computational modeling of AgNPs and their capping agents, with consideration of the metal core. Through molecular docking studies, the mechanism underlying the antiviral activity of these biogenic AgNPs was elucidated, facilitating a deeper understanding of the influence of the capping agents on the interaction between AgNPs and viral glycoproteins.

MATERIALS AND METHODS

Preparation of NPs. AgNPs with *J. regia* dried green husk aqueous extract and Ag/AgCl NPs using *M. sylvestris* leaf extracts were synthesized using methodologies described by Abbasi et al. (10) and Feizi et al. (11), respectively. 500 µg/mL of both NPs in distilled water, used as a dispersant, were prepared separately and stored in brown bottles at room temperature after 2 hrs of sonication. Also, iron oxide (Fe_3O_4) NPs were prepared using the co-reduction strategy, dried at 60°C for 2 hrs, and stored at room temperature until utilization (12).

Characterization of NPs. All samples were dispersed in Milli Q water to obtain suitable structural and thermodynamic wetting characteristics. Zeta potential measurements were carried out using a Malvern instrument at 25°C. The biosynthesized NPs were prepared at a concentration of 500 µg/mL in distilled water used as the dispersing medium, followed by sonication for 15 min prior to measurement. In a typical procedure, 60 µL of the AgNP suspension was mixed with 10 µL of 1 mM KCl solution and sonicated again for 15 minutes. The samples were analyzed without filtration (1).

Molecular docking. The Materials Studio 2017 software library served as the basis for the development of the Fe_3O_4 NPs, *M. sylvetris* AgNPs (M-AgNPs), and *J. regia* AgNPs (J-AgNPs) unit cells. The 3D structures of the NPs were then completed, opti-

mized, and energy-minimized using the steepest descent method in Avogadro. The optimized models of NPs can be downloaded in sdf format in the following link: https://drive.google.com/file/d/1g1CDbayn3-on-9i0KwQtJg8-WsM0JhiY5/view?usp=sharing.

The RCSB Protein Data Bank provided the PDB data for the 3D structures of the HSV-1 gD (PDB ID: 2C3A) and gL/gH (PDB ID: 3M1C) envelope glycoproteins. The interaction of two biomolecules, which are the most abundant chemicals in the aqueous extract of *J. regia* green husk and *M. sylvestris* leaves, Juglone and Quercetin, was also chosen to verify their roles in these biological interactions, as they may contribute as a capping agent. The protein structures of viruses were subjected to docking investigations using Molegro Virtual Docker (MVD), which removed water and ligand molecules from the structures. A protein-ligand docking simulation program called Molegro Virtual Docker determines the optimal shape of flexible ligands as they interact with proteins. After identifying the protein's binding site and the ligand's binding mode, the docking procedure was carried out. Ten docking sets were performed, and then the Nelder-Mead Simplex Minimization was used to minimize post-dock energy. Grid resolution was 0.30 Å. Ligand evaluation was based on the calculation of Internal ES, Internal HBond and Sp^2 Sp^2 torsions. The grid box radius was 15 Å. The grid box was set to X= 7.69, Y=30.81, and Z= -32.96 Å. Cavity docking volumes were 59.39 $Å^3$ for 2C3A and 143.46 $Å^3$ for 3M1C, respectively. Molegro Molecular Viewer 7.0 was used to examine the results and choose the optimum interaction position (13).

MVD uses four proprietary scoring functions and four search algorithms (14), and docking outcomes are assessed using the MolDock score. This score, derived from a specialized heuristic algorithm that combines differential evolution with cavity prediction, is commonly referred to as the E score. The MolDock score expands upon the piecewise linear potential (PLP) model by factoring in hydrogen bonding and electrostatic interactions (15), and it is determined through the accumulation of the energy components listed in Formula (1):

$$\text{MolDock (E score)} = E_{inter} + E_{intra}$$

E inter denotes the overall interaction energy, which reflects the interactions between the ligand and the protein, water, or any cofactors present. Conversely, E intra pertains to the internal energy of the ligand, encompassing electronic interactions, hydrogen bonding, steric effects, sp^2-sp^2 hybridization, torsional influences, van der Waals interactions, penalties from soft constraints, and solvation energy (E-solvation) (16).

MVD assesses and illustrates various forms of interactions, such as hydrogen bonds, electrostatic forces, and steric interactions between the ligand and specific amino acid residues within the protein. This evaluation offers a comprehensive overview of the critical forces that facilitate ligand-protein binding. For example, a hydrogen bond is a strong intermolecular or intramolecular interaction that arises when a hydrogen atom covalently bonded to a highly electronegative atom (such as oxygen, nitrogen, or fluorine) is attracted to the lone pair of another electronegative atom. Likewise, electrostatic interactions are the non-covalent forces that result in attraction or repulsion between charged particles, and they are essential in physics, chemistry, and biology, playing a significant role in molecular stability, protein folding, enzyme-substrate recognition, and various cellular processes. In molecular docking, steric interactions are repulsive forces that arise when atoms or groups of the ligand and the protein's binding site come too close in size, preventing unfavorable interactions and ensuring an appropriate fit for a stable complex. These interactions are vital for achieving shape complementarity, meaning the ligand's shape must align well with the binding site's cavity to form a stable, energy-minimized complex (17).

Cell culture. The Vero cell line was obtained from the Iranian Biological Resource Center (code C10001). Cells were cultured in Roswell Park Memorial Institute 1640 Medium (RPMI 1640 –Glutamax, Bioidea company, Tehran, Iran) supplemented with 10% fetal bovine serum (FBS, Gibco Invitrogen, Gaithersburg, MD, USA) and 1% Penicillin – Streptomycin Solution 100X (Bioidea company, Tehran, Iran) at 37°C in a 5% CO_2 atmosphere.

Virus propagation and quantifications. HSV-1 was obtained from the Iranian Blood Transfusion Organization (Virology Laboratory) and propagated in Vero cells. Viral titer was determined using the Reed and Muench method (18). Viral stock was stored at -70°C until further use.

MTT assay. The cells were cultured in 96-well microplates until they reached 80-90% confluence,

at which point they were ready to perform the test. Also, the highest 24-hour stable concentration of Ag-NPs was prepared from the stored stock and sonicated for 15 min. Several concentrations (5, 10, 20, 50, 80, 100, 150, and 200 µg/mL) of NPs were diluted in RPMI containing 20% FBS. Cells were incubated for 24 hrs at 37°C in 5% CO_2, after which the MTT assay (CIB Biotech, Tehran, Iran) was performed. Ten µL of MTT reagent was added to each well containing 100 µL of medium and incubated for 4 hrs. The supernatant was removed, and 100 µL of DMSO was added. Absorbance was measured at 750 nm following 30 min of incubation in the dark. In this way, the information was exported to Microsoft Excel, and a chart of cell viability and AgNPs concentration was generated (19).

Virus pre-treatment with Fe_3O_4 NPs and biosynthesized NPs. The Modeled virus was incubated with 300 µg/mL concentrations of biosynthesized NPs (prepared and sonicated for 15 min) for 1 hr (both biosynthesized NPs were used at the same concentration). Afterwards, samples were poured onto 300 mg of dried Fe_3O_4 NPs to achieve a concentration of 300 mg/mL (20). Samples were vortexed for 30 sec and sonicated at 37 kHz for 2 times, each taking 15 min. The supernatants were transferred into glass containers and placed in a shaker-incubator (WIS-20R, Daihan Scientific Co., Ltd., Korea) at 25°C, shaken at 0.3958 × g for 1 hr. After incubation at room temperature for 15 min, the samples were exposed to a neodymium magnet for 10 min, and the Fe_3O_4 NPs being biosynthesized NPs were separated. The achieved supernatants were drained and added to the medium to make a 10-fold dilution series (18). Treated viruses with only Fe_3O_4 NPs were represented as the Fe_3O_4 NPs antiviral activity control. Controls, prepared dilution series, and supernatants were added to a plate of Vero cells at 80% confluence and incubated for 24 hrs at 37ºC in 5% CO_2. After 24 hrs, the CPE effect was evaluated microscopically.

Field emission scanning electron microscopy (FESEM) of inactivated samples. Virus samples were incubated with biosynthesized NPs, then mixed with dried Fe_3O_4 NPs. The mixture was vortexed, sonicated, and magnetically separated to collect Fe_3O_4 NPs with adsorbed NPs. Supernatants were 10-fold diluted and applied to Vero cells for 24 hrs before CPE assessment. Samples were fixed with 4% glutaraldehyde buffer solution, then washed with 0.1 M phosphate buffer and dehydrated through different concentrations of ethanol (30, 50, 70, 80, 90, and 100%). Final preparations at Arya Electron Optics Co. were conducted utilizing the Electron Optic FESEM service. Observations were performed using the MAIA3 model of the FESEM electron microscope.

RESULTS

Characterization of NPs. The zeta potential of M-AgNPs and J-AgNPs was measured to be -5.49 mV and -8.87 mV, respectively (Fig. 1). These values indicate the surface charge of the synthesized NPs. The magnitude of the zeta potential indicates the stability of NP suspensions, with higher absolute values indicating greater repulsion between particles and a reduced likelihood of aggregation.

Molecular docking analysis. The interaction between the NP models and the glycoproteins of HSV-1 (gD and gL/gH) was investigated using MVD software. The docking scores (MolDock score), hydrogen bonds, steric interactions, and Root Mean Square Deviation (RMSD) for each interaction are summarized in Table 1. A MolDock score of approximately -170 was revealed for Fe_3O_4 NP in both interactions. Numerous hydrogen bonds were formed with gD, resulting in an RMSD of 1.342. Hydrogen bonds were not formed by Ag/AgCl NPs or Ag NPs; instead, only steric interactions were observed with certain residues. MolDock scores ranging from -40 to -25 were observed, along with reasonable RMSD values. High negative MolDock scores were shown by the Capping Agents (Juglone and Quercetin), indicating strong binding affinity. Specific residues involved in these interactions are presented in Fig. 2. Numerous hydrogen bonds were formed by Fe_3O_4 NPs with various residues due to the oxygen atoms in their structure, while steric interactions were simultaneously induced. In contrast, steric interactions were formed only by Ag and Ag/AgCl NPs with fewer residues. Furthermore, it was indicated that the chemical composition of the capping agents is a very significant factor in determining the anti-viral activity of a NP.

The docking results are shared via the following link: https://drive.google.com/file/d/14uYnzVEX-2jk4URP4czmbfCQD2PWkCr46/view?usp=sharing

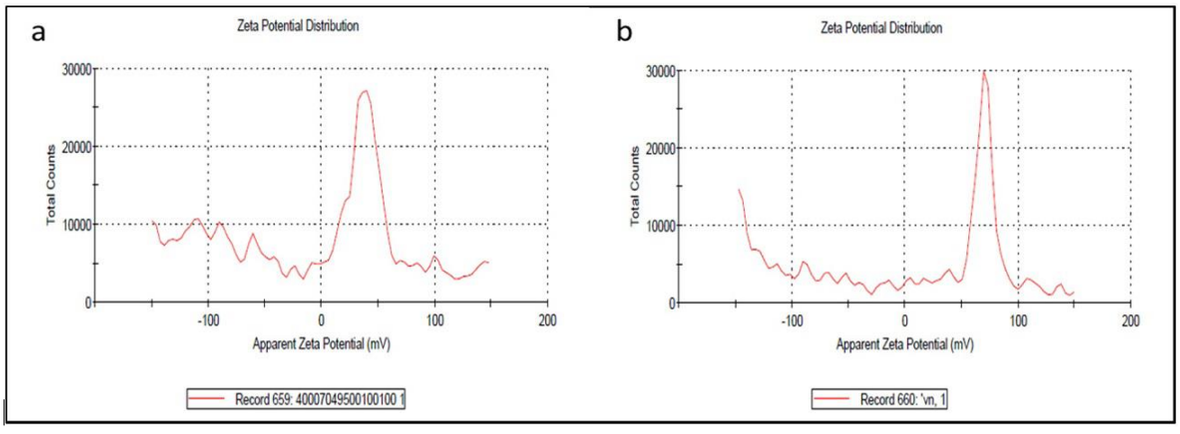

Fig. 1. Zeta potential distribution and surface measurement of a) M-AgNPs and b) J-AgNPs.

Table 1. The docking results of NPs and Juglone and Quecertin with HSV-1 glycoproteins and the involved amino acids residues.

Ligand	PDB ID	MolDock score	Hydrogen bond	Steric bond	RMSD
Fe_3O_4	2C3A	-170	Arg_{196}, Ser_{204}, Gln_{206}, Ala_{201}, Cys_{202}, Ser_{200}, Tyr_{137}, Leu_{203}, Ser_{204}, Arg_{101}, Arg_{105}, Ala_{201} and Glu_{159}	Pro_{199}, Pro_{198}, Gln_{206}, Leu_{62}, Arg_{184}, His_{183}, Ala_{157}, Leu_{195}, Pro_{51}, Pro_{50}, Asp_{172}, Leu_{181}, Ala_{161}, Cys_{202}, Tyr_{208}, Gly_{63}, Ala_{201} and Ile_{108}	1.342
	3M1C	-168	Asn_{670}, Asn_{670}, Thr_{703}, Ser_{656}, Cys_{706} and Thr_{705}	Ser_{656}, Cys_{706}, Thr_{705}, Asn_{670}, Pro_{681}, Thr_{668}, Asn_{653}, Arg_{711}, Thr_{703}, Pro_{655}, Ala_{710} and Ser_{653}	2.562
Ag/AgCl	2C3A	-29	-	Glu_{117}, Thr_{116} and Cys_{302}	3.671
	3M1C	-37	-	Asn_{658}, Arg_{642} and Asn_{638}	3.231
Ag	2C3A	-38	-	Cys_{302}, Thr_{116} and Ile_{40}	2.678
	3M1C	-25	-	Arg_{682}, His_{657}, Leu_{680}, Asn_{658} and Pro_{681}	1.671
Juglone	2C3A	-60	Tyr_{38}, Cys_{302} and His_{39}	Tyr_{38}, Cys_{302} and His_{39}	0.345
	3M1C	-62	Thr_{700}, Leu_{680}	Gly_{683}, Gly_{685}, Pro_{679} and Leu_{680}	1.345
Quecertin	2C3A	-73	His_{39}, Tyr_{38} and Cys_{302}	Tyr_{38}, His_{39}, Ala_{303} and Cys_{302}	3.789
	3M1C	-100	Arg_{424}, Arg_{416}, Tyr_{637}	Arg_{481}, Arg_{416}, Leu_{436}, Val_{434}, Ala_{431}, Tyr_{637}	2.456

Cytotoxicity of AgNPs on the Vero cell line. The Maximum Non-Toxic Dose (MNTD) of J-AgNPs was determined to be 10 µg/mL. For M-AgNPs, which exhibited higher toxicity, the MNTD was 5 µg/mL (Fig. 3). Cell viability was maintained at concentrations below the MNTD. Notably, significant increases in cell viability were observed exclusively at lower concentrations (5 and 2.5 µg/mL).

Antiviral activity of Fe^3O^4 NPs and biosynthesized NPs. Due to the high toxicity and low MNTD of AgNPs, direct antiviral assays were ineffective at safe concentrations. Therefore, an indirect assay was employed to assess antiviral properties. Antiviral activity tests were performed using the 50% Tissue Culture Infection Dose per mL technique (Fig. 4). Fe_3O_4 NPs demonstrated inherent antiviral activity;

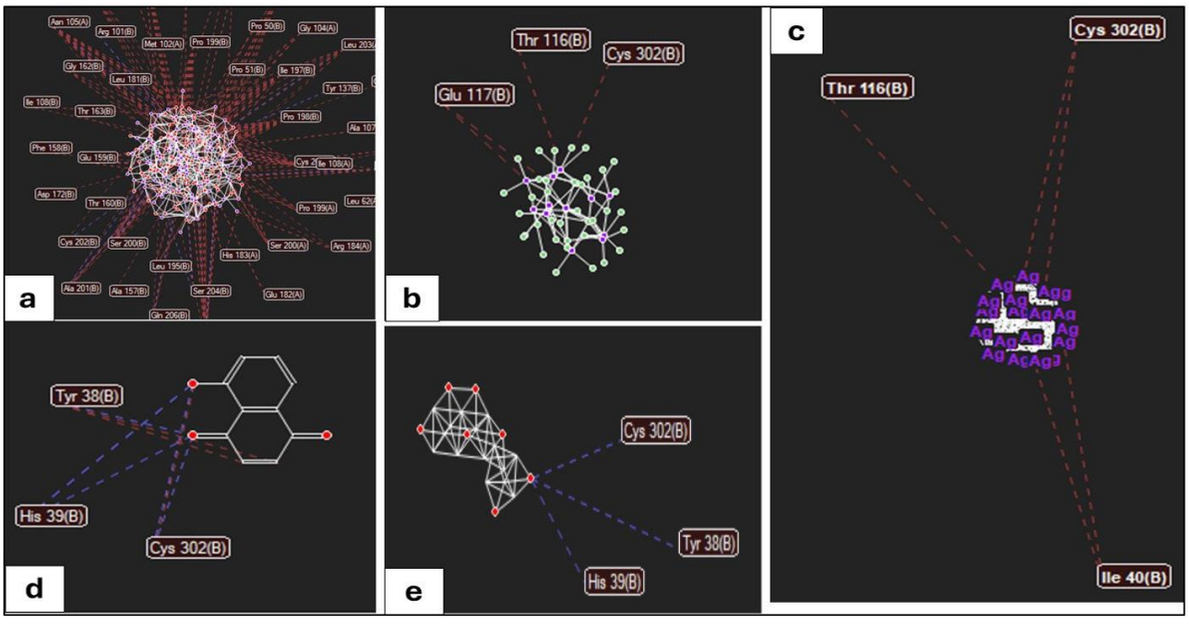

Fig. 2. The docking interactions of Fe_3O_4 NPs (a), Ag/AgCl NPs (b), AgNPs (c), Jugone (d) and Quecertin (e) with gD glycoprotein. Blue and red dashes indicate for the hydrogen and steric bonds between the ligands and the residues respectively.

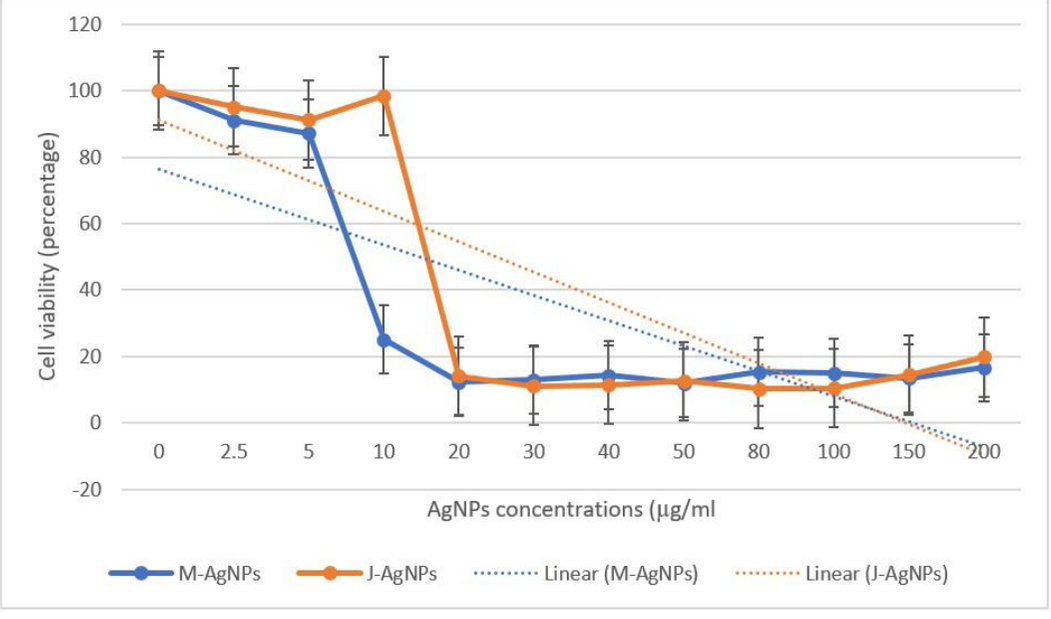

Fig. 3. Cell viability in MTT test after exposure to M-AgNPs and J-AgNPs concentrations. Each concentration has repeated 3 times.

when combined with high concentrations of biosynthesized NPs, they enhanced overall virucidal activity. The viral titers of the modeled viruses after various treatments are detailed in Table 2. The exact concentrations of both biosynthesized NPs were used in the assays, alongside equal concentrations of Fe_3O_4 NPs.

FESEM of treated samples. FESEM images were obtained from samples containing HSV-1 treated with Fe_3O_4 NPs, HSV-1 treated with J-AgNPs and Fe_3O_4 NPs, and HSV-1 treated with M-AgNPs and Fe_3O_4 NPs. As shown in Fig. 5, NPs were observed on the surface of HSV-1 virions, providing visual evidence supporting the docking study's findings.

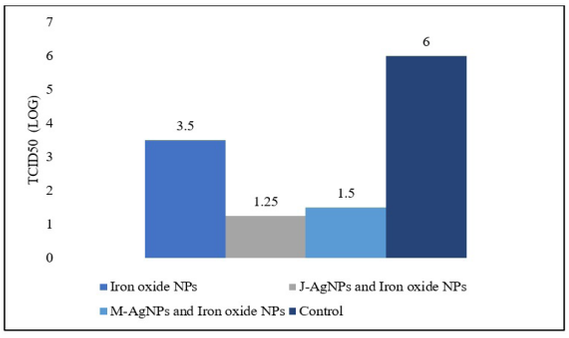

Fig. 4. The antiviral activity of Fe_3O_4 NPs and biosynthesized NPs against HSV-1 was evaluated. The HSV-1 titer was expressed in a logarithmic scale, with untreated HSV-1 serving as the control.

Table 2. Modeled virus titer after being treated with Fe O NPs and biosynthesized NPs. Concentration of Fe O NPs, J-AgNPs and M-AgNPs in all tests were 300 mg/mL, 300 µg/mL and 300 µg/mL, respectively.

Treatment	HSV-1 titer
Fe O NPs	$10^{3.5}$
J-AgNPs and Fe O NPs	$10^{1.25}$
M-AgNPs and Fe O NPs	$10^{1.5}$

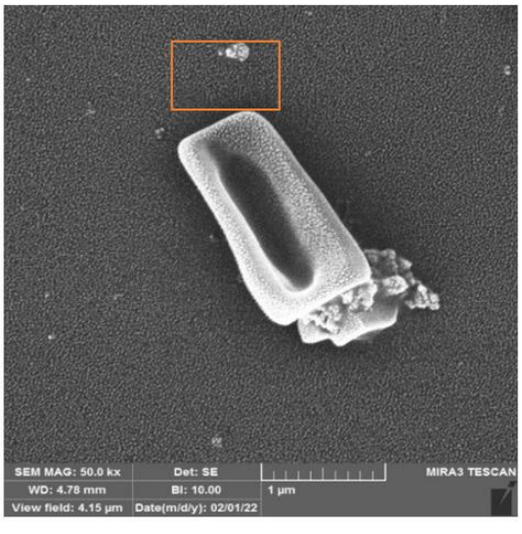

Fig. 5. FESEM image of HSV-1 after being treated with AgNPs and Fe O NPs.

DISCUSSION

The current study investigated the physicochemical characterization, cytotoxicity, and antiviral mechanisms of biosynthesized AgNPs and magnetite Fe O NPs against HSV-1.

Stability and surface charge. The zeta potential values obtained (-5.49 mV for M-AgNPs and -8.87 mV for J-AgNPs) provide insight into the stability of the NP suspensions. A higher magnitude of zeta potential (positive or negative) typically indicates greater repulsion between particles, leading to increased stability and reduced aggregation risk. Conversely, lower magnitudes suggest weaker repulsion and a higher risk of aggregation. Therefore, zeta potential analysis is a valuable tool for controlling the stability of nanomaterial suspensions, which is crucial for biomedical applications (21).

The zeta potential of AgNPs varies with particle size and surface coating. In this study, the capping agents were plant-derived extracts. The zeta potential indicates the surface charge of AgNPs and has been shown to positively correlate with antiviral effects, offering a novel perspective for understanding their mechanism (22). The electric double layer surrounding the NPs, consisting of the surface charge, Stern layer, and diffuse layer, is essential for colloidal stability (Fig. 6). This layer contributes significantly to the NPs' antimicrobial and antiviral activities (23-25).

DISCUSSION

Both plant-derived AgNPs demonstrated notable antiviral activity against HSV 1, with viral titers reduced by more than 10^4. Their low zeta potential facilitated closer interactions with viral particles by minimizing electrostatic repulsion. The slightly higher zeta potential of M-AgNPs may account for the minor variation in their antiviral efficacy.

Furthermore, the small particle size of both AgNPs contributed to enhanced viral interaction. Molecular docking analyses confirmed that juglone and quercetin, essential phytochemicals within the capping agents, exhibit strong binding affinity to HSV 1 glycoprotein D through hydrogen bonding and steric interactions. The metallic core appears to amplify these effects synergistically. J-AgNP's slightly smaller size and positive charge may underlie its slightly better antiviral activity.

Taken together, the results suggest that these AgNPs inhibit HSV 1 attachment and penetration, a mechanism further supported by FESEM observations.

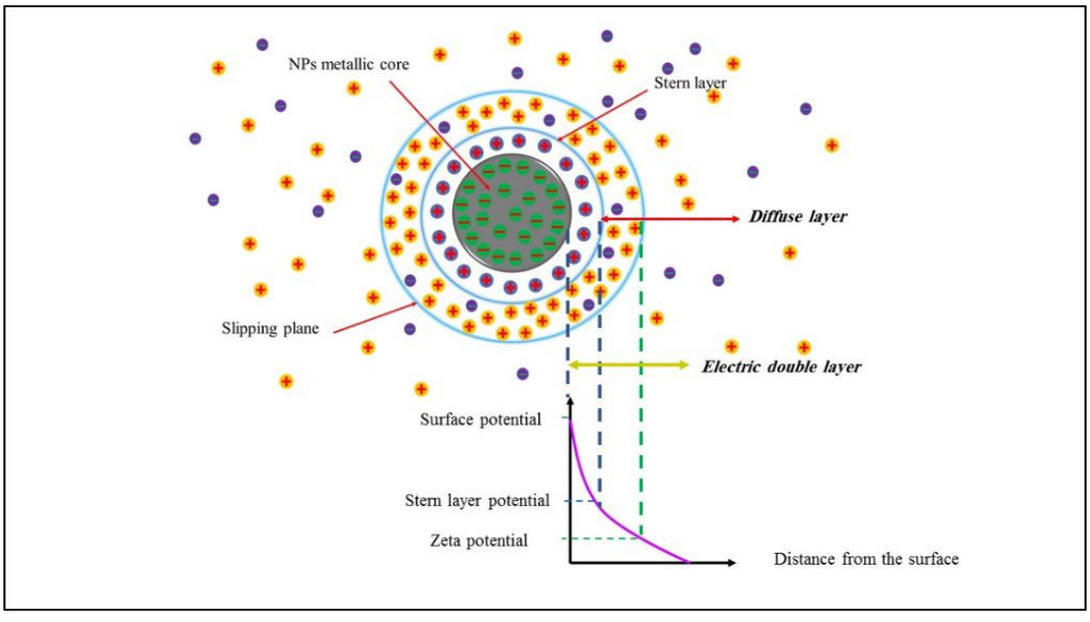

Fig. 6. The electric double layer of a NP.

Molecular docking and mechanism of action. Since the chemical composition of NPs consists of both the metal core and the capping agent, the interactions of the most abundant compounds in the extracts—Juglone (from *J. regia* green husk) and Quercetin (from *M. sylvestris* leaves)—with HSV-1 glycoproteins (gD and gL/gH) were investigated.

The docking results revealed that Fe_3O_4 NPs exhibited the most potent inhibitory properties, with a MolDock score of -170 and numerous hydrogen bonds with gD (RMSD: 1.342). This suggests severe inhibition and blockade of the viral protein. In contrast, Ag and Ag/AgCl NPs showed lower MolDock scores (-40 to -25) and formed only steric interactions, indicating less stable binding. However, the capping agents (Juglone and Quercetin) showed high negative MolDock scores, suggesting that the phytochemicals play a significant role in viral inhibition. Two key inferences can be drawn from these data:

1. Metal oxide NPs (such as Fe_3O_4) exhibit more potent inhibitory properties than metal NPs (such as AgNPs) due to the presence of oxygen atoms, which facilitate hydrogen bonding.

2. The chemical composition of the capping agent is a critical determinant of the antiviral activity of the resulting NP.

Size-dependent virucidal activity. AgNPs possess large specific surface areas inversely proportional to their diameter. Smaller AgNPs have more surface atoms, increasing the number of available adsorption and bonding sites for foreign species. Previous studies have shown that the virucidal action of AgNPs is size-dependent, with smaller NPs exhibiting greater activity (26). In this study, the average sizes of J-AgNPs and M-AgNPs were 7 nm and 25 nm, respectively, which are significantly smaller than the HSV-1 particle size (155–240 nm) (27). This size difference allows NPs to maneuver between viral particles and engage with them effectively.

Interaction with viral glycoproteins and cell entry. HSV-1 cellular entry relies on interactions between envelope glycoproteins and heparan sulfate (HS) moieties on cell surfaces. AgNPs can mimic HS and interact with HSV-1, impeding viral contact with host cells (28). Additionally, tannic acid-modified AgNPs have been shown to interfere with cell attachment by interacting with viral glycoproteins (29). Our findings suggest that biosynthesized AgNPs interact with HSV-1 glycoproteins, disrupting attachment.

Their electrical charge influences the cellular uptake and efficacy of AgNPs. Cationic AgNPs generally exhibit greater cellular uptake than anionic or neutral counterparts. However, in the context of virucidal activity, negative zeta potential values (associated with lower toxicity) create an electrostatic

barrier that impedes virus-particle interactions. Conversely, less negative or positive zeta potentials (e.g., in PVP- or BPEI-coated AgNPs) exhibit heightened toxicity due to diminished repulsion (1, 21). A study on SARS-CoV-2 (which shares envelope similarities with HSV-2) also reported a positive correlation between zeta potential and virucidal efficacy (22).

Comparison with biosynthesized NPs. Previous studies on mycosynthesized AgNPs against HSV-1 indicated that AgNPs regulate viral infectivity by impeding virus-cell interactions, a process influenced by size and zeta potential (8, 30). For instance, AgNPs derived from *F. oxysporum* and *Curvularia* species (4–23 nm) demonstrated superior antiviral activity (80%–90% inhibition) against HSV-1 with lower cytotoxicity. Our findings align with these results, suggesting that the antiviral efficacy of plant-extract-derived NPs is comparable to previously reported biosynthesized NPs. This similarity is attributed to the close zeta potentials and mean sizes of the NPs, which the capping agents determine, while the metallic core contributes synergistically.

Cytotoxicity and reactive oxygen species generation. The MNTD for J-AgNPs was 10 µg/mL, while M-AgNPs showed higher toxicity with an MNTD of 5 µg/mL. The cytotoxicity of AgNPs is often attributed to oxidative stress. AgNPs can induce the production of reactive oxygen species (ROS), deplete antioxidants, and inhibit antioxidant enzymes, leading to DNA damage and cell death. There is a documented relationship between ROS generation, autophagy, and apoptosis. Excess ROS can alter autophagy, causing organelle damage (including mitochondria), inflammation, and oxidative stress (25). The cytotoxicity assay in this study was crucial to confirm that the antiviral effects observed at lower concentrations were not merely artifacts of cell death, thereby ensuring the validity of the subsequent antiviral tests.

FESEM observations and proposed mechanism. FESEM images confirmed the presence of NPs on the surface of HSV-1 virions (Fig. 5), supporting the docking study results. The exact mechanism by which AgNPs exert virucidal effects is multifaceted (Fig. 7). They may prevent infection by blocking the virus's entry into host cells or by directly inactivating it. Potential mechanisms include binding to viral coat proteins to disrupt structural integrity, binding to the viral surface to degrade genomic material or prevent entry, hindering interaction with the cell membrane, inhibiting the interaction between viral nucleocapsids and cellular components, interacting with viral genomic material (e.g., HBV dsDNA) to inhibit replication, and disrupting cellular processes such as protein synthesis.

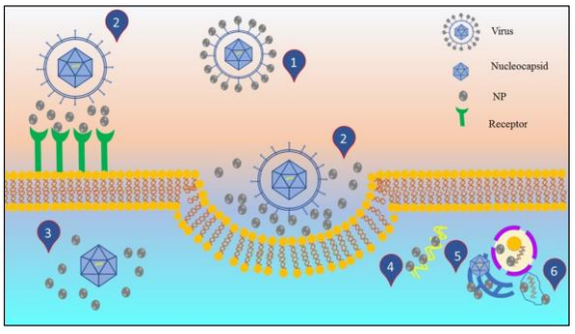

Fig. 7. Suggested AgNPs mechanisms of action: 1. Virus inhibition by binding with the glycoproteins; 2. Interface viral attachment by interacting with the specific receptors on the host cells; 3. Suppression of cellular signaling pathways of the virus; 4. Interaction with the virus's genome; 5. Viral genome replication repression; 6. Inhibit cellular factors vital for viral replication.

Our results suggest that the primary mechanism of action for the NPs in this study involves direct viral inactivation through engagement with viral glycoproteins, thereby interrupting viral attachment and penetration.

CONCLUSION

Both plant-derived AgNPs demonstrated notable antiviral activity against HSV 1, with viral titers reduced by more than 10^4. Their low zeta potential facilitated closer interactions with viral particles by minimizing electrostatic repulsion. The slightly higher zeta potential of M-AgNPs may account for the minor variation in their antiviral efficacy. Furthermore, the small particle size of both AgNPs contributed to enhanced viral interaction. Molecular docking analyses confirmed that juglone and quercetin, essential phytochemicals within the capping agents, exhibit strong binding affinity to HSV 1 glycoprotein D through hydrogen bonding and steric interactions. The metallic core appears to amplify these effects synergistically. J-AgNP's slightly smaller size and positive charge may underlie its slightly

better antiviral activity. Taken together, the results suggest that these AgNPs inhibit HSV 1 attachment and penetration, a mechanism further supported by FESEM observations.

ACKNOWLEDGEMENTS

We gratefully thank Dr. Zohreh Sharifi for providing us with HSV-1 sample.

REFERENCES

1. Sinclair TR, van den Hengel SK, Raza BG, Rutjes SA, de Roda Husman AM, Peijnenburg WJGM, et al. Surface chemistry-dependent antiviral activity of silver nanoparticles. *Nanotechnology* 2021; 32. doi: 10.1088/1361-6528/ac03d6.
2. Morens DM, Folkers GK, Fauci AS. The challenge of emerging and re-emerging infectious diseases. *Nature* 2004; 430: 242-249.
3. Luceri A, Francese R, Lembo D, Ferraris M, Balagna C. Silver Nanoparticles: Review of Antiviral Properties, Mechanism of Action and Applications. *Microorganisms* 2023; 11: 629.
4. Kausar S, Said Khan F, Ishaq Mujeeb Ur Rehman M, Akram M, Riaz M, Rasool G, et al. A review: Mechanism of action of antiviral drugs. *Int J Immunopathol Pharmacol* 2021; 35: 20587384211002621.
5. Zhu S, Viejo-Borbolla A. Pathogenesis and virulence of herpes simplex virus. *Virulence* 2021; 12: 2670-2702.
6. Sharmin S, Rahaman MM, Sarkar C, Atolani O, Islam MT, Adeyemi OS. Nanoparticles as antimicrobial and antiviral agents: A literature-based perspective study. *Heliyon* 2021; 7(3): e06456.
7. Liaqat N, Jahan N, Khalil-Ur-Rahman, Anwar T, Qureshi H. Green synthesized silver nanoparticles: Optimization, characterization, antimicrobial activity, and cytotoxicity study by hemolysis assay. *Front Chem* 2022; 10: 952006.
8. Aletayeb P, Ghadam P, Mohammadi P. Green synthesis of AgCl/Ag(3)PO(4) nanoparticle using cyanobacteria and assessment of its antibacterial, colorimetric detection of heavy metals and antioxidant properties. *IET Nanobiotechnol* 2020; 14: 707-713.
9. Zhao J, Wang X, Hoang SA, Bolan NS, Kirkham MB, Liu J, et al. Silver nanoparticles in aquatic sediments: Occurrence, chemical transformations, toxicity, and analytical methods. *J Hazard Mater* 2021; 418: 126368.
10. Abbasi Z, Feizi S, Taghipour E, Ghadam P. Green synthesis of silver nanoparticles using aqueous extract of dried *Juglans regia* green husk and examination of its biological properties. *Green Process Synth* 2017; 6: 477-485.
11. Feizi S, Taghipour E, Ghadam P, Mohammadi P. Antifungal, antibacterial, antibiofilm and colorimetric sensing of toxic metals activities of eco friendly, economical synthesized Ag/AgCl nanoparticles using Malva Sylvestris leaf extracts. *Microb Pathog* 2018; 125: 33-42.
12. Ayadi Hassan S, Gorji V, Ghadam P. The efficient magnetic separation of the four biogenic nanoparticles from aqueous media by the unmodified iron oxide nanoparticles. *Int J Environ Sci Technol* 2021; 18: 3883-3894.
13. Ahmadi M, Elikaei A, Ghadam P. Antiviral activity of biosynthesized copper nanoparticle by *Juglans regia* green husk aqueous extract and Iron nanoparticle: molecular docking and in-vitro studies. *Iran J Microbiol* 2023; 15: 138-148.
14. Bitencourt-Ferreira G, de Azevedo WF Jr. Molegro Virtual Docker for Docking. *Methods Mol Biol* 2019; 2053: 149-167.
15. Thomsen R, Christensen MH. MolDock: a new technique for high-accuracy molecular docking. *J Med Chem* 2006; 49: 3315-3321.
16. Dubey K, Dubey R. Computation screening of narcissoside a glycosyloxyflavone for potential novel coronavirus 2019 (COVID-19) inhibitor. *Biomed J* 2020; 43: 363-367.
17. Qiu B, Shao Q, Shi J, Yang C, Chu H. Application of biochar for the adsorption of organic pollutants from wastewater: Modification strategies, mechanisms and challenges. *Sep Purif Technol* 2022; 300: 121925.
18. Lei C, Yang J, Hu J, Sun X. On the calculation of TCID50 for quantitation of virus infectivity. *Virol Sin* 2021; 36: 141-144.
19. Ramalingam V, Rajaram R, Premkumar C, Santhanam P, Dhinesh P, Vinothkumar S, et al. Biosynthesis of silver nanoparticles from deep sea bacterium *Pseudomonas aeruginosa* JQ989348 for antimicrobial, antibiofilm, and cytotoxic activity. *J Basic Microbiol* 2014; 54: 928-936.
20. Mwilu SK, Siska E, Baig RBN, Varma RS, Heithmar E, Rogers KR. Separation and measurement of silver nanoparticles and silver ions using magnetic particles. *Sci Total Environ* 2014; 472: 316-323.
21. Lunardi CN, Gomes AJ, Rocha FS, De Tommaso J, Patience GS. Experimental methods in chemical engineering: Zeta potential. *Can J Chem Eng* 2021; 99: 627-639.
22. He Q, Lu J, Liu N, Lu W, Li Y, Shang C, et al. Antiviral Properties of Silver Nanoparticles against SARS-CoV-2: Effects of Surface Coating and Particle Size. *Nanomaterials (Basel)* 2022; 12: 990.

23. Liang T, Hou JR, Qu M, Xi JX, Raj I. Application of nanomaterial for enhanced oil recovery. *Pet Sci* 2022; 19: 882-899.
24. Park SJ, Seo MK (2011). Intermolecular Force. In: Interface Science and Composites. Elsevier, pp. 1-57.
25. Al-kawmani AA, Alanazi KM, Farah MA, Ali MA, Hailan WA, Al-Hemaid FM. Apoptosis-inducing potential of biosynthesized silver nanoparticles in breast cancer cells. *J King Saud Univ Sci* 2020; 32: 2480-2488.
26. Dove AS, Dzurny DI, Dees WR, Qin N, Nunez Rodriguez CC, Alt LA, et al. Silver nanoparticles enhance the efficacy of aminoglycosides against antibiotic-resistant bacteria. *Front Microbiol* 2023; 13: 1064095.
27. Laine RF, Albecka A, Linde S Van De, Rees EJ, Crump CM, Kaminski CF. Structural analysis of herpes simplex virus by optical super-resolution imaging. *Nat Commun* 2015; 6: 5980.
28. Ratan ZA, Mashrur FR, Chhoan AP, Shahriar SM, Haidere MF, Runa NJ, et al. Silver Nanoparticles as Potential Antiviral Agents. *Pharmaceutics* 2021; 13: 2034.
29. Salleh A, Naomi R, Utami ND, Mohammad AW, Mahmoudi E, Mustafa N, et al. The potential of silver nanoparticles for antiviral and antibacterial applications: a mechanism of action. *Nanomaterials (Basel)* 2020; 10: 1566.
30. Gaikwad S, Ingle A, Gade A, Rai M, Falanga A, Incoronato N, et al. Antiviral activity of mycosynthesized silver nanoparticles against herpes simplex virus and human parainfluenza virus type 3. *Int J Nanomed* 2013; 8: 4303-4314.